Measurement of the B_S^0 meson lifetime using semileptonic decays

F. Abe,[17] H. Akimoto,[39] A. Akopian,[31] M. G. Albrow,[7] A. Amadon,[5] S. R. Amendolia,[27] D. Amidei,[20] J. Antos,[33]
S. Aota,[37] G. Apollinari,[31] T. Arisawa,[39] T. Asakawa,[37] W. Ashmanskas,[18] M. Atac,[7] P. Azzi-Bacchetta,[25] N. Bacchetta,[25]
S. Bagdasarov,[31] M. W. Bailey,[22] P. de Barbaro,[30] A. Barbaro-Galtieri,[18] V. E. Barnes,[29] B. A. Barnett,[15] M. Barone,[9]
G. Bauer,[19] T. Baumann,[11] F. Bedeschi,[27] S. Behrends,[3] S. Belforte,[27] G. Bellettini,[27] J. Bellinger,[40] D. Benjamin,[35]
J. Bensinger,[3] A. Beretvas,[7] J. P. Berge,[7] J. Berryhill,[5] S. Bertolucci,[9] S. Bettelli,[27] B. Bevensee,[26] A. Bhatti,[31]
K. Biery,[7] C. Bigongiari,[27] M. Binkley,[7] D. Bisello,[25] R. E. Blair,[1] C. Blocker,[3] S. Blusk,[30] A. Bodek,[30] W. Bokhari,[26]
G. Bolla,[29] Y. Bonushkin,[4] D. Bortoletto,[29] J. Boudreau,[28] L. Breccia,[2] C. Bromberg,[21] N. Bruner,[22] R. Brunetti,[2]
E. Buckley-Geer,[7] H. S. Budd,[30] K. Burkett,[20] G. Busetto,[25] A. Byon-Wagner,[7] K. L. Byrum,[1] M. Campbell,[20]
A. Caner,[27] W. Carithers,[18] D. Carlsmith,[40] J. Cassada,[30] A. Castro,[25] D. Cauz,[36] A. Cerri,[27] P. S. Chang,[33] P. T. Chang,[33]
H. Y. Chao,[33] J. Chapman,[20] M. -T. Cheng,[33] M. Chertok,[34] G. Chiarelli,[27] C. N. Chiou,[33] F. Chlebana,[7]
L. Christofek,[13] M. L. Chu,[33] S. Cihangir,[7] A. G. Clark,[10] M. Cobal,[27] E. Cocca,[27] M. Contreras,[5] J. Conway,[32] J. Cooper,[7]
M. Cordelli,[9] D. Costanzo,[27] C. Couyoumtzelis,[10] D. Cronin-Hennessy,[6] R. Culbertson,[5] D. Dagenhart,[38] T. Daniels,[19]
F. DeJongh,[7] S. Dell'Agnello,[9] M. Dell'Orso,[27] R. Demina,[7] L. Demortier,[31] M. Deninno,[2] P. F. Derwent,[7] T. Devlin,[32]
J. R. Dittmann,[6] S. Donati,[27] J. Done,[34] T. Dorigo,[25] N. Eddy,[20] K. Einsweiler,[18] J. E. Elias,[7] R. Ely,[18]
E. Engels, Jr.,[28] W. Erdmann,[7] D. Errede,[13] S. Errede,[13] Q. Fan,[30] R. G. Feild,[41] Z. Feng,[15] C. Ferretti,[27] I. Fiori,[2]
B. Flaugher,[7] G. W. Foster,[7] M. Franklin,[11] J. Freeman,[7] J. Friedman,[19] Y. Fukui,[17] S. Gadomski,[14] S. Galeotti,[27]
M. Gallinaro,[26] O. Ganel,[35] M. Garcia-Sciveres,[18] A. F. Garfinkel,[29] C. Gay,[41] S. Geer,[7] D. W. Gerdes,[15] P. Giannetti,[27]
N. Giokaris,[31] P. Giromini,[9] G. Giusti,[27] M. Gold,[22] A. Gordon,[11] A. T. Goshaw,[6] Y. Gotra,[28] K. Goulianos,[31]
H. Grassmann,[36] L. Groer,[32] C. Grosso-Pilcher,[5] G. Guillian,[20] J. Guimaraes da Costa,[15] R. S. Guo,[33] C. Haber,[18] E. Hafen,[19]
S. R. Hahn,[7] R. Hamilton,[11] T. Handa,[12] R. Handler,[40] F. Happacher,[9] K. Hara,[37] A. D. Hardman,[29] R. M. Harris,[7]
F. Hartmann,[16] J. Hauser,[4] E. Hayashi,[37] J. Heinrich,[26] W. Hao,[35] B. Hinrichsen,[14] K. D. Hoffman,[29] M. Hohlmann,[5]
C. Holck,[26] R. Hollebeek,[26] L. Holloway,[13] Z. Huang,[20] B. T. Huffman,[28] R. Hughes,[23] J. Huston,[21] J. Huth,[11] H. Ikeda,[37]
M. Incagli,[27] J. Incandela,[7] G. Introzzi,[27] J. Iwai,[39] Y. Iwata,[12] E. James,[20] H. Jensen,[7] U. Joshi,[7] E. Kajfasz,[25]
H. Kambara,[10] T. Kamon,[34] T. Kaneko,[37] K. Karr,[38] H. Kasha,[41] Y. Kato,[24] T. A. Keaffaber,[29] K. Kelley,[19] R. D. Kennedy,[7]
R. Kephart,[7] D. Kestenbaum,[11] D. Khazins,[6] T. Kikuchi,[37] B. J. Kim,[27] H. S. Kim,[14] S. H. Kim,[37] Y. K. Kim,[18]
L. Kirsch,[3] S. Klimenko,[8] D. Knoblauch,[16] P. Koehn,[23] A. Köngeter,[16] K. Kondo,[37] J. Konigsberg,[8] K. Kordas,[14] A. Korytov,[8]
E. Kovacs,[1] W. Kowald,[6] J. Kroll,[26] M. Kruse,[30] S. E. Kuhlmann,[1] E. Kuns,[32] K. Kurino,[12] T. Kuwabara,[37]
A. T. Laasanen,[29] S. Lami,[27] S. Lammel,[7] J. I. Lamoureux,[3] M. Lancaster,[18] M. Lanzoni,[27] G. Latino,[27] T. LeCompte,[1]
S. Leone,[27] J. D. Lewis,[7] M. Lindgren,[4] T. M. Liss,[13] J. B. Liu,[30] Y. C. Liu,[33] N. Lockyer,[26] O. Long,[26] C. Loomis,[32]
M. Loreti,[25] D. Lucchesi,[27] P. Lukens,[7] S. Lusin,[40] J. Lys,[18] K. Maeshima,[7] P. Maksimovic,[11] M. Mangano,[27]
M. Mariotti,[25] J. P. Marriner,[7] G. Martignon,[25] A. Martin,[41] J. A. J. Matthews,[22] P. Mazzanti,[2] K. McFarland,[30] P. McIntyre,[34]
P. Melese,[31] M. Menguzzato,[25] A. Menzione,[27] E. Meschi,[27] S. Metzler,[26] C. Miao,[20] T. Miao,[7] G. Michail,[11] R. Miller,[21]
H. Minato,[37] S. Miscetti,[9] M. Mishina,[17] S. Miyashita,[37] N. Moggi,[27] E. Moore,[22] Y. Morita,[17] A. Mukherjee,[7]
T. Muller,[16] P. Murat,[27] S. Murgia,[21] M. Musy,[36] H. Nakada,[37] T. Nakaya,[5] I. Nakano,[12] C. Nelson,[7] D. Neuberger,[16]
C. Newman-Holmes,[7] C.-Y. P. Ngan,[19] L. Nodulman,[1] A. Nomerotski,[8] S. H. Oh,[6] T. Ohmoto,[12] T. Ohsugi,[12] R. Oishi,[37]
M. Okabe,[37] T. Okusawa,[24] J. Olsen,[40] C. Pagliarone,[27] R. Paoletti,[27] V. Papadimitriou,[35] S. P. Pappas,[41] N. Parashar,[27]
A. Parri,[9] J. Patrick,[7] G. Pauletta,[36] M. Paulini,[18] A. Perazzo,[27] L. Pescara,[25] M. D. Peters,[18] T. J. Phillips,[6] G. Piacentino,[27]
M. Pillai,[30] K. T. Pitts,[7] R. Plunkett,[7] A. Pompos,[29] L. Pondrom,[40] J. Proudfoot,[1] F. Ptohos,[11] G. Punzi,[27] K. Ragan,[14]
D. Reher,[18] M. Reischl,[16] A. Ribon,[25] F. Rimondi,[2] L. Ristori,[27] W. J. Robertson,[6] T. Rodrigo,[27] S. Rolli,[38] L. Rosenson,[19]
R. Roser,[13] T. Saab,[14] W. K. Sakumoto,[30] D. Saltzberg,[4] A. Sansoni,[9] L. Santi,[36] H. Sato,[37] P. Schlabach,[7]
E. E. Schmidt,[7] M. P. Schmidt,[41] A. Scott,[4] A. Scribano,[27] S. Segler,[7] S. Seidel,[22] Y. Seiya,[37] F. Semeria,[2] T. Shah,[19]
M. D. Shapiro,[18] N. M. Shaw,[29] P. F. Shepard,[28] T. Shibayama,[37] M. Shimojima,[37] M. Shochet,[5] J. Siegrist,[18] A. Sill,[35]
P. Sinervo,[14] P. Singh,[13] K. Silwa,[38] C. Smith,[15] F. D.Snider,[15] J. Spalding,[7] T. Speer,[10] P. Sphicas,[19] F. Spinella,[27]
M. Spiropulu,[11] L. Spiegel,[7] L. Stanco,[25] J. Steele,[40] A. Stefanini,[27] R. Ströhmer,[7,*] J. Strologas,[13] F. Strumia,[10] D. Stuart,[7]
K. Sumorok,[19] J. Suzuki,[37] T. Suzuki,[37] T. Takahashi,[24] T. Takano,[24] R. Takashima,[12] K. Takikawa,[37] M. Tanaka,[37]
B. Tannenbaum,[22] F. Tartarelli,[27] W. Taylor,[14] M. Tecchio,[20] P. K. Teng,[33] Y. Teramoto,[24] K. Terashi,[37] S. Tether,[19]
D. Theriot,[7] T. L. Thomas,[22] R. Thurman-Keup,[1] M. Timko,[38] P. Tipton,[30] A. Titov,[31] S. Tkaczyk,[7] D. Toback,[5]
K. Tollefson,[30] A. Tollestrup,[7] H. Toyoda,[24] W. Trischuk,[14] J. F. de Troconiz,[11] S. Truitt,[20] J. Tseng,[19] N. Turini,[27]
T. Uchida,[37] F. Ukegawa,[26] J. Valls,[32] S. C. van den Brink,[28] S. Vejcik III,[20] G. Velev,[27] R. Vidal,[7] R. Vilar,[7,*] D. Vucinic,[19]
R. G. Wagner,[1] R. L. Wagner,[7] J. Wahl,[5] N. B. Wallace,[27] A. M. Walsh,[32] C. Wang,[6] C. H. Wang,[33] M. J. Wang,[33]
A. Warburton,[14] T. Watanabe,[37] T. Watts,[32] R. Webb,[34] C. Wei,[6] H. Wenzel,[16] W. C. Wester III,[7] A. B. Wicklund,[1]
E. Wicklund,[7] R. Wilkinson,[26] H. H. Williams,[26] P. Wilson,[5] B. L. Winer,[23] D. Winn,[20] D. Wolinski,[20] J. Wolinski,[21]
S. Worm,[22] X. Wu,[10] J. Wyss,[27] A. Yagil,[7] W. Yao,[18] K. Yasuoka,[37] G. P. Yeh,[7] P. Yeh,[33] J. Yoh,[7] C. Yosef,[21]
T. Yoshida,[24] I. Yu,[7] A. Zanetti,[36] F. Zetti,[27] and S. Zucchelli[2]

(CDF Collaboration)

^{1}Argonne National Laboratory, Argonne, Illinois 60439

^{2}Istituto Nazionale di Fisica Nucleare, University of Bologna, I-40127 Bologna, Italy

^{3}Brandeis University, Waltham, Massachusetts 02254

^{4}University of California at Los Angeles, Los Angeles, California 90024

^{5}University of Chicago, Chicago, Illinois 60637

^{6}Duke University, Durham, North Carolina 27708

^{7}Fermi National Accelerator Laboratory, Batavia, Illinois 60510

^{8}University of Florida, Gainesville, Florida 32611

^{9}Laboratori Nazionali di Frascati, Istituto Nazionale di Fisica Nucleare, I-00044 Frascati, Italy

^{10}University of Geneva, CH-1211 Geneva 4, Switzerland

^{11}Harvard University, Cambridge, Massachusetts 02138

^{12}Hiroshima University, Higashi-Hiroshima 724, Japan

^{13}University of Illinois, Urbana, Illinois 61801

^{14}Institute of Particle Physics, McGill University, Montreal, Canada H3A 2T8

and University of Toronto, Toronto, Canada M5S 1A7

^{15}The Johns Hopkins University, Baltimore, Maryland 21218

^{16}Institut für Experimentelle Kernphysik, Universität Karlsruhe, D-76128 Karlsruhe, Germany

^{17}National Laboratory for High Energy Physics (KEK), Tsukuba, Ibaraki 305, Japan

^{18}Ernest Orlando Lawrence Berkeley National Laboratory, Berkeley, California 94720

^{19}Massachusetts Institute of Technology, Cambridge, Massachusetts 02139

^{20}University of Michigan, Ann Arbor, Michigan 48109

^{21}Michigan State University, East Lansing, Michigan 48824

^{22}University of New Mexico, Albuquerque, New Mexico 87131

^{23}The Ohio State University, Columbus, Ohio 43210

^{24}Osaka City University, Osaka 588, Japan

^{25}Universita di Padova, Istituto Nazionale di Fisica Nucleare, Sezione di Padova, I-35131 Padova, Italy

^{26}University of Pennsylvania, Philadelphia, Pennsylvania 19104

^{27}Istituto Nazionale di Fisica Nucleare, University and Scuola Normale Superiore of Pisa, I-56100 Pisa, Italy

^{28}University of Pittsburgh, Pittsburgh, Pennsylvania 15260

^{29}Purdue University, West Lafayette, Indiana 47907

^{30}University of Rochester, Rochester, New York 14627

^{31}Rockefeller University, New York, New York 10021

^{32}Rutgers University, Piscataway, New Jersey 08855

^{33}Academia Sinica, Taipei, Taiwan 11530, Republic of China

^{34}Texas A&M University, College Station, Texas 77843

^{35}Texas Tech University, Lubbock, Texas 79409

^{36}Istituto Nazionale di Fisica Nucleare, University of Trieste/Udine, Italy

^{37}University of Tsukuba, Tsukuba, Ibaraki 315, Japan

^{38}Tufts University, Medford, Massachusetts 02155

^{39}Waseda University, Tokyo 169, Japan

^{40}University of Wisconsin, Madison, Wisconsin 53706

^{41}Yale University, New Haven, Connecticut 06520

The lifetime of the B_S^0 meson is measured using the semileptonic decay $B_S^0 \rightarrow D_S^- l^+ \nu X$. The data sample consists of about 110 pb^{-1} of $p\bar{p}$ collisions at $\sqrt{s} = 1.8$ TeV collected by the CDF detector at Fermilab. Four different D_S^- decay modes are reconstructed resulting in approximately 600 $D_S^- l^+$ signal events. The B_S^0 meson lifetime is determined to be $\tau(B_S^0) = (1.36 \pm 0.09^{+0.06}_{-0.05})$ ps, where the first and second uncertainties are statistical and systematic, respectively. The B_S^0 meson decay length distribution is examined for a lifetime difference $\Delta\Gamma/\Gamma$ between the two mass eigenstates of the B_S^0 meson. An upper limit of $\Delta\Gamma/\Gamma < 0.83$ is set at the 95% confidence level. [S0556-2821(99)01103-0]

I. INTRODUCTION

The lifetime differences between different bottom flavored hadrons probe B decay mechanisms which are beyond the simple quark spectator model. In the case of charm me-

sons, such differences have been observed to be quite large $[\tau(D^+)/\tau(D^0) \sim 2.5]$ [1]. Among bottom hadrons, the lifetime differences are expected to be smaller due to the heavier bottom quark mass [2,3]. Some QCD inspired models based on the heavy quark expansion [2] predict a difference be-

tween the B^+ and B^0 meson lifetimes of about 5% but expect the B^0 and B_S^0 lifetimes to differ by no more than 1%. Although some assumptions in Ref. [2] have been questioned in Ref. [3], there is agreement that the models expect a difference between the B^0 and B_S^0 lifetimes of less than about 1%. These predictions are consistent with previous results of the B^0 and B^+ meson lifetimes, as well as recent B_S^0 lifetime measurements [1,4,5].

In the standard model [6], the B_S^0 meson exists in two CP-conjugate states, $|B_S^0\rangle = |\bar{b}s\rangle$ and $|\bar{B}_S^0\rangle = |b\bar{s}\rangle$. The two mass eigenstates of the B_S^0 meson, B_S^H and $B_S^L (H=$ ''heavy'' and $L=$ ''light''), are not CP eigenstates but are mixtures of the two CP-conjugate quark states:

$$|B_S^H\rangle = p\,|B_S^0\rangle - q\,|\bar{B}_S^0\rangle, \quad |B_S^L\rangle = p\,|B_S^0\rangle + q\,|\bar{B}_S^0\rangle,$$
$$\text{with } p^2 + q^2 = 1. \quad (1)$$

The mass and lifetime differences between the B_S^H and B_S^L can be defined as

$$\Delta m \equiv m_H - m_L, \quad \Delta\Gamma \equiv \Gamma_L - \Gamma_H, \quad \Gamma = \frac{\Gamma_H + \Gamma_L}{2}, \quad (2)$$

where $m_{H,L}$ and $\Gamma_{H,L}$ denote the mass and decay width of B_S^H and B_S^L. Unlike in the case of the B^0 meson, the width difference in the B_S^0 system is expected to be large [7]. Theoretical estimates predict $\Delta\Gamma/\Gamma$ to be on the order of 10%–20% [8,9]. In the B_S^0 system the ratio $\Delta m/\Delta\Gamma$ is related to the ratio of the Cabibbo-Kobayashi-Maskawa (CKM) [10] matrix elements $|V_{cb}V_{cs}|/|V_{ts}V_{tb}|$, which is quite well known, and depends only on QCD corrections within the standard model [9,11]. Currently these QCD corrections are known to next-to-leading order in the $1/m_b$ expansion [9]. A measurement of $\Delta\Gamma$ would therefore imply a determination of Δm and thus a way to infer the existence of B_S^0 meson oscillations, which will ultimately determine the ratio of the CKM matrix elements $|V_{td}|/|V_{ts}|$.

It is assumed that B_S^0 mesons are produced as an equal mixture of B_S^H and B_S^L [9]. In a search for $\Delta\Gamma$, the B_S^0 meson decay length distribution can be described by a function of the form

$$\mathcal{F}(t) = e^{-\Gamma_H t} + e^{-\Gamma_L t} \quad \text{with } \Gamma_{L,H} = \Gamma \pm \Delta\Gamma/2, \quad (3)$$

rather than by just one exponential lifetime $e^{-\Gamma t}$ which is the functional form used in the measurement of the B_S^0 lifetime assuming a single lifetime.

In this paper, we present an update of the B_S^0 lifetime measurement at the Collider Detector at Fermilab (CDF) [5] using the semileptonic decay[1] $B_S^0 \rightarrow D_S^- l^+ \nu X$ $(l=e,\mu)$, where the D_S^- is identified via the four decay modes $D_S^- \rightarrow \phi\pi^-, K^{*0}K^-, K_S^0 K^-$, and $\phi\mu^-\nu$. We also examine the B_S^0 decay length distribution for a lifetime difference $\Delta\Gamma/\Gamma$

---

[1]Throughout the paper references to a specific charge state imply the charge-conjugate state as well.

with a fit to two exponential lifetimes. The data sample consists of approximately 110 pb^{-1} of $p\bar{p}$ collisions at $\sqrt{s}$ $=1.8$ TeV collected with the CDF detector during Run I. Of this, approximately 20 pb^{-1} were collected during the 1992-1993 running period, while about 90 pb^{-1} were accumulated during the 1994-1996 run of the Fermilab Tevatron Collider. The result presented in this paper supersedes CDF's previous measurement of the B_S^0 lifetime using semileptonic B_S^0 decays [5]. That publication was based on 20 pb^{-1} of data and reconstructed the D_S^- meson in the $\phi\pi^-$ decay mode only.

The outline of this article is as follows: After a short description of the CDF detector in Sec. II, the selection of the $D_S^- l^+$ candidates is detailed in Sec. III. The determination of the B_S^0 lifetime is the topic of Sec. IV. We describe the search for a lifetime difference $\Delta\Gamma/\Gamma$ in Sec. V and offer our conclusions in Sec. VI.

II. CDF DETECTOR

The CDF experiment is a multi-purpose detector designed to study 1.8 TeV $p\bar{p}$ collisions produced by the Fermilab Tevatron Collider. The detector has a coordinate system with the z-axis along the proton beam direction, the y-axis pointing vertically upwards, and the x-axis pointing horizontally out of the Tevatron ring. Throughout this article φ is the azimuthal angle, θ is the polar angle measured from the proton direction, and r is the radius perpendicular to the beam axis. The CDF detector is described in detail elsewhere [12]. We summarize here only the detector features most relevant to this analysis.

Three devices inside the 1.4 T solenoidal magnetic field are used for the tracking of charged particles: the silicon vertex detector (SVX), a set of vertex time projection chambers (VTX), and the central tracking chamber (CTC). The SVX [13] consists of four layers of silicon microstrip detectors located at radii between 2.9 cm and 7.9 cm from the interaction point. It provides spatial measurements in the r-φ plane with a track impact parameter resolution of about $(13 + 40/p_T)$ μm [13], where p_T is the component of the track momentum p transverse to the z-axis $(p_T = p\sin\theta)$ given in GeV/c. The geometric acceptance of the SVX is about 60% as it covers only ± 25 cm from the nominal interaction point whereas the luminous region of the Tevatron beam has a rms of ~ 30 cm along the beam direction.

The VTX, which is located outside the SVX up to a radius of 22 cm, reconstructs track segments in the r-z plane and is used to determine the z-position of the primary interaction vertex with a resolution of about 0.2 cm on average. Surrounding the SVX and VTX is the CTC, located between radii of 30 cm and 132 cm. The CTC is a 3.2 m long cylindrical drift chamber that contains 84 layers of sense wires grouped into nine alternating super-layers of axial and stereo wires with a stereo angle of 3°. The outer 54 layers of the CTC are instrumented to record the specific ionization dE/dx of charged particles. The CTC covers the pseudorapidity interval $|\eta|$ less than about 1.1, where $\eta = -\ln[\tan(\theta/2)]$. The p_T resolution of the CTC combined with the SVX is

$\sigma(p_T)/p_T = [(0.0066)^2 + (0.0009\,p_T)^2]^{1/2}$, with p_T measured in GeV/c.

Outside the solenoid are electromagnetic (CEM) and hadronic (CHA) calorimeters ($|\eta| < 1.1$) that employ a projective tower geometry with a segmentation of $\Delta\eta \times \Delta\varphi \sim 0.1 \times 15°$. The sampling medium is composed of scintillators layered with lead and steel absorbers. A layer of proportional wire chambers (CES) is located near shower maximum in the CEM and provides a measurement of electromagnetic shower profiles in both the φ- and z-directions.

The muon detection system has four of its layers of planar drift chambers (CMU) located beyond the central calorimeters. To reduce the probability of misidentifying penetrating hadrons as muon candidates in the pseudorapidity region $|\eta| \leq 0.6$, four more layers of chambers (CMP) are located outside the magnet return yoke. To reach these two detectors, particles produced at the primary interaction vertex with a polar angle of 90° must traverse material totaling 5.4 and 8.4 pion interaction lengths, respectively. An additional set of muon chambers (CMX) is located in the pseudorapidity interval $0.6 < |\eta| < 1.0$ to extend the polar acceptance of the muon system.

III. DATA SELECTION

In this section, we describe the data selection, which begins with the description of the lepton trigger data sets. This is followed by a summary of the selection requirements, which are applied to obtain the $D_S^- l^+$ candidate events used for the B_S^0 lifetime measurements. At the end of this section, we briefly describe the Monte Carlo simulation of our data.

A. Lepton trigger data

Events containing semileptonic B_S^0 decays are collected using inclusive electron and muon trigger data as well as a data set obtained from a dimuon trigger. CDF uses a three-level trigger system. The first two levels are hardware based triggers, while level 3 is a software trigger based on the offline reconstruction code optimized for computational speed.

At level 1, inclusive electrons are selected by the presence of a single calorimeter tower above a threshold of 6–8 GeV depending on run conditions, while inclusive muons require the presence of a track in the CMU as well as the CMP. At level 2, both of these triggers demand a charged track with $p_T > 7.5$ GeV/c reconstructed in the r-φ plane of the CTC by the central fast tracker (CFT) [14], a hardware track processor, which uses fast timing information from the CTC as input. The momentum resolution of the CFT is $\sigma(p_T)/p_T^2 = 3.5\%$ with a high efficiency. In the case of the electron trigger, this track has to be matched to a cluster in the electromagnetic calorimeter with transverse energy $E_T > 8.0$ GeV, where $E_T = E \sin\theta$, with E being the energy of the calorimeter cluster. In the case of the muon trigger, this track must be matched to a reconstructed track-segment in both the CMU and CMP. At level 3, a computer farm is used to fully reconstruct the data including three-dimensional track reconstruction in the CTC. However, the fast algorithm

used for tracking is only efficient for particles with $p_T > 1.4$ GeV/c. In the third level of the trigger more stringent electron and muon selection criteria, which are similar to those described in the next Sec. III B, are applied.

The reconstruction of the $D_S^- \to \phi\mu^-\nu$ decay mode is based on dimuon trigger data where the level 1 trigger requires two muon candidates be observed in the muon system. The second level trigger requires the detection of at least one CFT track with $p_T > 2$ GeV/c to match in φ of each muon candidate. The third level trigger requires that two reconstructed CTC tracks be matched with two tracks in the muon chambers and the dimuon invariant mass be less than 2.8 GeV/c^2. During Run I about 7.5×10^6 electron trigger events and about 2.5×10^6 inclusive muon trigger events were recorded by CDF, while about 1.3×10^6 dimuon trigger events with a dimuon invariant mass of less than 2.8 GeV/c^2 were recorded.

B. Lepton identification

The identification of electron candidates reconstructed after data collection uses information from both the calorimeters and the tracking chambers. The longitudinal shower profile has to be consistent with an electron shower with a leakage energy from the CEM into the CHA of less than 4% if one track is pointing to the calorimeter tower or less than 10% if more than one track is pointing to the calorimeter tower. The lateral shower profile of the CEM cluster has to be consistent with that from test beam electrons. Additionally, a χ^2 comparison of the CES shower profile with that of test beam electrons has to result in $\chi^2 < 10$. For the association of a single high p_T track with the calorimeter shower based on the position matching at the CES plane, it is required that $r|\Delta\varphi| < 1.5$ cm and $|\Delta z \sin\theta| < 3$ cm. In addition, we demand the E_T of the electron candidate reconstructed offline to be greater than 6 GeV. Electron candidates from photon conversion due to detector material are reduced to less than 10% by looking for oppositely charged tracks which have a small opening angle with the electron candidate.

The reconstruction of muon candidates is described in Ref. [15]. We compute a χ^2 characterizing the separation between the track segment in the muon chamber and the extrapolated CTC track, where the uncertainty in this χ^2 variable is dominated by the multiple scattering in the detector material. We require $\chi^2 < 9$ in the r-φ view (CMU, CMP, and CMX) and $\chi^2 < 12$ in the r-z view (CMU and CMX). The transverse muon momentum reconstructed off line is required to be $p_T > 6$ GeV/c. For the dimuon sample this cut is $p_T > 2$ GeV/c for each muon candidate. Finally, for optimal vertex resolution the electron and muon candidate tracks have to be reconstructed in the SVX detector.

C. D_S^- selection

The D_S^- candidates are reconstructed in the decay modes
(i) $D_S^- \to \phi\pi^-$, $\phi \to K^+K^-$,
(ii) $D_S^- \to K^{*0}K^-$, $K^{*0} \to K^+\pi^-$,
(iii) $D_S^- \to K_S^0 K^-$, $K_S^0 \to \pi^+\pi^-$,

(iv) $D_S^- \to \phi \mu^- \nu$, $\phi \to K^+ K^-$.

The D_S^- reconstruction is explained in the next section with the example of the $\phi \pi^-$ decay channel. The other D_S^- decay channels (ii)–(iv) are reconstructed in a similar way. We then describe only the differences in the selection of these decays (ii)–(iv) as compared to the $D_S^- \to \phi \pi^-$ decay mode. The kinematic selection criteria used in this analysis are optimized by maximizing the quantity $N_S / \sqrt{N_S + N_B}$, where N_S is the predicted number of signal events based on Monte Carlo calculations (see Sec. III D) and N_B is the observed number of background events estimated from the D_S^- sideband regions (see Sec. IV E).

1. $D_S^- \to \phi \pi^-$ mode

The $D_S^- \to \phi \pi^-$ reconstruction starts with a search for $\phi \to K^+ K^-$ candidates. We first define a search cone around the lepton candidate with a radius $\Delta R = \sqrt{(\Delta \eta)^2 + (\Delta \varphi)^2}$ of 0.8. Any two oppositely charged tracks with $p_T > 1.2$ GeV/c within that cone are assigned the kaon mass and combined to form a ϕ candidate. Each ϕ candidate is required to have a mass within ± 10 MeV/c^2 of the world average ϕ mass [1]. The ϕ candidate is then combined with another track of $p_T > 0.8$ GeV/c inside the cone which has the opposite charge of the lepton (we call this the ''right-sign'' combination). This third track is assigned the pion mass. To ensure a good decay vertex measurement, track quality cuts requiring a minimum number of hits in the CTC are imposed on the tracks forming the D_S^- candidate. In addition, each of the tracks forming the D_S^- is required to be reconstructed in the SVX with hits in at least three out of the four silicon layers and the χ^2 of the track fit per SVX hit has to be less than 6 to reject badly measured tracks. The same track selection requirements are also applied to the lepton candidate tracks.

The specific ionization information dE/dx from the CTC is used to help identify hadrons in the D_S^- reconstruction. Because of the large Landau tail of the ionization distribution, the 80% truncated mean of the measured charges from the CTC sense wires is taken as the best estimator of the track dE/dx. The probabilities, $P(i)$, for a track to be consistent with the $i = e, \mu, \pi, K,$ or p hypotheses are then calculated using the measured dE/dx value and the predictions for the assumed particle hypotheses. We define a likelihood ratio, $lh_{dE/dx}^K$, for a track being a kaon to be the ratio of $P(K)$ divided by the sum of the probabilities of all particle hypotheses. The quantity $lh_{dE/dx}^\pi$ is defined correspondingly. We require the likelihood ratios $lh_{dE/dx}^K > 0.01$ and $lh_{dE/dx}^\pi > 0.01$.

Since the ϕ has spin 1 and both the D_S^- and π^- are spin 0, the helicity angle Ψ, which is the angle between the K^- and D_S^- directions in the ϕ rest frame, exhibits a distribution $dN/d(\cos \Psi) \sim \cos^2 \Psi$. A cut $|\cos \Psi| > 0.4$ is therefore applied to suppress the combinatorial background, which is found to be flat in the $\cos \Psi$ distribution. We also apply an isolation cut $E_T^{iso}/p_T(\phi \pi^-) < 1.0$ on the D_S^- candidate, where E_T^{iso} is the sum of the transverse energy within a cone of radius 0.4 in η-φ space around the lepton candidate, excluding the lep-
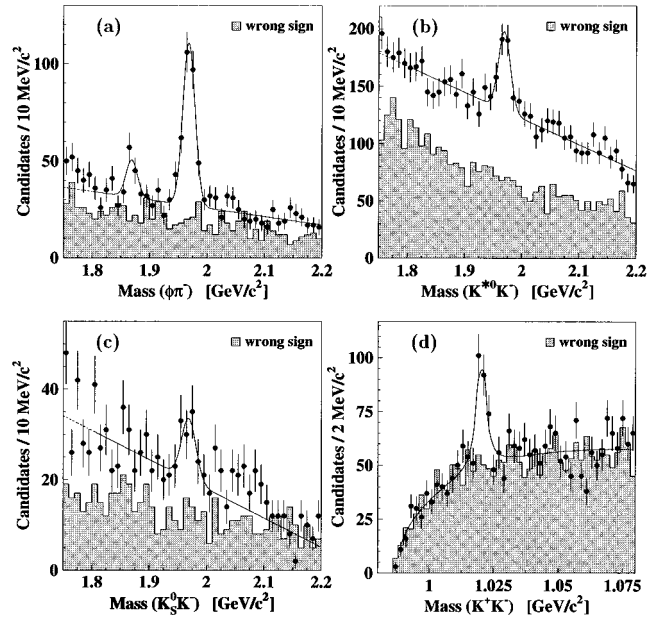

FIG. 1. Invariant mass distributions of (a) $D_S^- \to \phi \pi^-$, (b) $D_S^- \to K^{*0} K^-$, (c) $D_S^- \to K_S^0 K^-$, and (d) $\phi \to K^+ K^-$ from $D_S^- \to \phi \mu^- \nu$. The dots with error bars are for ''right-sign'' $D_S^- l^+$ combinations while the shaded histograms show the corresponding ''wrong-sign'' distributions. In (a) evidence of the decay $D^- \to \phi \pi^-$ is present. The results of the fits described in the text are also superimposed. The mass regions indicated by a dashed line have not been included in the fits.

ton energy. This cut eliminates many of the fake D_S^- combinations from high track multiplicity jets. Finally, the mass of the $D_S^- l^+$ system is required to be between 3.0 GeV/c^2 and 5.0 GeV/c^2 to be consistent with coming from a B_S^0 decay.

In Fig. 1(a) the $\phi \pi^-$ invariant mass distribution for the ''right-sign'' $D_S^- l^+$ combinations is displayed. A D_S^- signal of 220 ± 21 events is observed from fitting a Gaussian with a mean of (1968 ± 1) MeV/c^2 and a width of (10.5 ± 1.1) MeV/c^2 plus a straight line to describe the combinatorial background. The mass region indicated by a dashed line has not been included in the fit to avoid contributions from D_S^- decays where particles have been missed such as the π^0 in the decay $D_S^- \to \phi \pi^- \pi^0$. Evidence of the Cabibbo-suppressed decay $D^- \to \phi \pi^-$ is also present in Fig. 1(a). The shaded distribution shows $\phi \pi^-$ candidates from ''wrong-sign'' $D_S^- l^-$ combinations. Here, no enhancement is seen in the D_S^- mass region. We allow multiple $\phi \pi^-$ combinations per event but the number of multiple entries is found to be less than 1% of the total number of combinations. This is also the case for the $D_S^- \to K^{*0} K^-$ and $K_S^0 K^-$ decay modes.

2. $D_S^- \to K^{*0} K^-$ mode

For the $D_S^- \to K^{*0} K^-$ decay mode with $K^{*0} \to K^+ \pi^-$, we assign the K^+ and π^- masses to two oppositely charged tracks found in the cone of $\Delta R < 0.8$ around the lepton. To reflect the different decay kinematics of the $K^{*0} \to K^+ \pi^-$ decay compared to $\phi \to K^+ K^-$, we require $p_T(K^+) > 1.2$ GeV/c and $p_T(\pi^-) > 0.4$ GeV/c. Each K^{*0} candidate

is required to have a mass within ± 40 MeV/c^2 of the world average K^{*0} mass [1]. To further reduce the high combinatorial background in this decay channel, we tighten the helicity cut to $|\cos \Psi| > 0.5$ and introduce a track based isolation requirement $p_{\mathrm{T}}(D_S^- l^+)/p_{\mathrm{T}}(\mathrm{cone}) > 0.6$, where $p_{\mathrm{T}}(\mathrm{cone})$ is the sum of the transverse momenta of all tracks in a cone $\Delta R < 1.0$ in η-ϕ space. The cone has the lepton direction as its axis and the primary event vertex (see Sec. IV A) as its vertex. All other selection requirements discussed in the $\phi \pi^-$ decay mode remain the same with the exception of the $lh_{\mathrm{d}E/\mathrm{d}x}^{K^-}$ cut described below.

The $K^{*0}K^-$ invariant mass distribution for the ''right-sign'' $D_S^- l^+$ combinations is shown as dots with error bars in Fig. 1(b). A signal at the D_S^- mass is visible. This signal contains also events from a $D^- \to K^{*0}\pi^-$ reflection, where the π^- is incorrectly assigned the kaon mass. This reflection is further discussed in Sec. IV C. To reduce the effect of this reflection the dE/dx requirement for that track is tightened to $lh_{\mathrm{d}E/\mathrm{d}x}^{K^-} > 0.1$, while we still demand $lh_{\mathrm{d}E/\mathrm{d}x}^{\pi,K} > 0.01$ for the tracks forming the K^{*0} candidate.

3. $D_S^- \to K_S^0 K^-$ mode

The reconstruction of the $D_S^- \to K_S^0 K^-$ decay mode begins with a search for $K_S^0 \to \pi^+ \pi^-$ candidates by assigning the pion mass to any two oppositely charged tracks with $p_{\mathrm{T}} > 0.4$ GeV/c in a cone of $\Delta R < 1.0$ in η-ϕ space around the lepton. These two tracks are constrained to come from a common vertex and their invariant mass has to be within 5σ of the nominal K_S^0 mass [1], where σ is the uncertainty on the $\pi^+ \pi^-$ mass measurement. Exploiting the long lifetime of the K_S^0 meson, we require the K_S^0 vertex to be significantly displaced from the primary event vertex, which is further described in Sec. IV A. We determine the transverse decay length L_{xy} (see Sec. IV B) of the K_S^0 and require $L_{\mathrm{xy}} > 3\sigma$, where σ is the measured uncertainty on L_{xy} for each candidate event.

The K_S^0 candidate is combined with any kaon candidate with $p_{\mathrm{T}} > 1.2$ GeV/c within $\Delta R < 0.8$ around the lepton to find the D_S^- candidate. The dots with error bars in Fig. 1(c) show the $K_S^0 K^-$ invariant mass distribution for the ''right-sign'' $D_S^- l^+$ combinations. An enhancement at the D_S^- mass is visible. As in the $K^{*0}K^-$ mode, this signal contains events from a $D^- \to K_S^0 \pi^-$ reflection, where the π^- is assigned the kaon mass (see Sec. IV C). To reduce the effect of this reflection, we again require $lh_{\mathrm{d}E/\mathrm{d}x}^{K^-} > 0.1$, while we demand $lh_{\mathrm{d}E/\mathrm{d}x}^{\pi} > 0.01$ for the tracks forming the K_S^0.

4. $D_S^- \to \phi \mu^- \nu$ mode

For the $D_S^- \to \phi \mu^- \nu$ decay mode, we start with two oppositely charged muons with $p_{\mathrm{T}} > 2$ GeV/c utilizing the dimuon data set obtained with a trigger which requires the dimuon invariant mass to be smaller than 2.8 GeV/c^2. This requirement is more than 90% efficient for a double semileptonic decay $B_S^0 \to D_S^- \mu^+ \nu X$ followed by $D_S^- \to \phi \mu^- \nu$. In addition, two oppositely charged tracks with $p_{\mathrm{T}} > 0.8$ GeV/c are assigned the kaon mass and combined to form a ϕ candidate. There is an ambiguity in the assignment of one of the two muons to a found $\phi \to K^+ K^-$ candidate. One of the muons comes from the D_S^- semileptonic decay ($\mu_{D_S^-}$) while the other originates from the B_S^0 decay ($\mu_{B_S^0}$). In order to resolve this ambiguity, we require m($KK\mu_{D_S^-}$) to be smaller than the world average D_S^- mass [1], while m($KK\mu_{B_S^0}$) has to be greater than m$_{D_S^-}$. To reduce combinatorial background in this decay channel, we use the track based isolation quantity $p_{\mathrm{T}}(D_S^- l^+)/p_{\mathrm{T}}(\mathrm{cone})$ and require it to be greater than 0.5. As required in the other decay modes, the invariant mass of the $KK\mu\mu$ system has to lie between 3.0 GeV/c^2 and 5.0 GeV/c^2. The number of multiple $D_S^- \mu^+$ combinations per event is larger compared to the other three decay modes (about 10%). We therefore allow only one D_S^- candidate per event by choosing the $D_S^- \mu^+$ combination with the largest probability from the combined vertex fit (see Sec. IV B).

The $K^+ K^-$ invariant mass distribution for the $D_S^- \mu^+$ sample is shown in Fig. 1(d) with the fit result overlaid. To obtain the number of ϕ signal events, we fit a second order polynomial together with a Breit-Wigner line shape convoluted with a Gaussian to account for detector resolution. We find 205 ± 38 ϕ signal events and measure the ϕ mass to be (1020.1 ± 0.5)MeV/c^2 in agreement with the world average ϕ mass [1]. The shaded histogram in Fig. 1(d) shows the ''wrong-sign'' KK mass spectrum, where we consider events with same sign $K^\pm K^\pm$ or $\mu^\pm \mu^\pm$ combinations as ''wrong-sign.'' For display purposes the ''wrong-sign'' distribution is scaled by a factor of 0.6 to the same area as the combinatorial background of the ''right-sign'' $K^+ K^-$ distribution. The ''wrong-sign'' distribution describes very well the shape of the combinatorial $K^+ K^-$ background. No indication of a ϕ signal is evident in the ''wrong-sign'' distribution.

D. Monte Carlo simulation

Some quantities in this analysis like efficiencies or the K-factor distribution further described in Sec. IV B are determined using a Monte Carlo (MC) calculation of b quark production and B meson decay followed by a simulation of the detector response to the final state particles. Since we extract only kinematic quantities of the B hadron decay from this Monte Carlo study, we do not simulate the underlying event from the $p\bar{p}$ scattering or include fragmentation products, but generate only B hadrons and their decay products.

The MC simulation begins with a model of b quark production based on a next-to-leading order QCD calculation [16]. This calculation employs the Martin-Roberts-Stirling set D0 (MRSD0) parton distribution function [17] to model the kinematics of the initial state partons. We generate b quarks in the rapidity interval $|y_b| < 1.0$ with a minimum p_{T} for the b quark of 8 GeV/c and 5 GeV/c to simulate events corresponding to the single lepton and dimuon data samples, respectively. These p_{T} requirements are chosen in a way to avoid any biases in the B meson kinematic distributions after the application of the kinematic cuts used in the analysis. The b quarks are fragmented into B mesons according to a model using the fragmentation function of Peterson

et al. [18] with a Peterson parameter of $\epsilon_b = 0.006$. The bottom and charm hadrons are decayed into the various final states using branching ratios and decay kinematics governed by the world average masses and lifetimes of the involved particles [1].

Events with a lepton above a momentum threshold corresponding to the appropriate hardware trigger are kept based on an efficiency parametrization of the CFT trigger that depends on the lepton p_T. The accepted events are passed through a simulation of the CDF detector that is based on parametrizations and simple models of the detector response, which are functions of the particle kinematics. After the simulation of the CDF detector, the same selection criteria applied to the data are imposed on the Monte Carlo events.

IV. B_S^0 LIFETIME ANALYSIS

In this section, we describe the measurement of the B_S^0 lifetime starting with the determination of the primary event vertex followed by the reconstruction of the B_S^0 decay length. In order to determine the number of D_S^- signal events used as a constraint in the lifetime fit, a reflection from D^- decays has to be considered for the $D_S^- \rightarrow K^{*0} K^-$ and $D_S^- \rightarrow K_S^0 K^-$ decay modes. In Sec. IV D background from non-B_S^0 decays is discussed, while the lifetime fit is detailed in Sec. IV E. The B_S^0 lifetime fit results are then presented together with the determination of the systematic uncertainties.

A. Primary event vertex

The B_S^0 lifetime reported in this paper is based on measuring the distance between the primary $p\bar{p}$ event vertex and the secondary B_S^0 decay vertex in the transverse plane. We first identify the z-position of the primary interaction vertex using the tracks reconstructed in the VTX detector. These tracks, when projected back to the beam axis, determine the longitudinal location of the primary interaction with an accuracy of about 0.2 cm along the beam direction. The primary vertices are distributed along the beam direction according to a Gaussian function with a width of ~30 cm. On average during Run I, the number of reconstructed interaction vertices in a given event follows a Poisson distribution with a mean of about 2.5. For the B_S^0 lifetime measurement, we determine the z-location of the primary event vertex by choosing the $p\bar{p}$ interaction vertex recorded by the VTX which is closest to the intercept of the lepton from the semileptonic B_S^0 decay with the beam line. We also require the z-coordinates of all tracks from the D_S^- decay to be within 5 cm of the z-coordinate of this primary vertex.

The transverse position of the primary event vertex is determined by using the average beam position through the detector together with the knowledge of the longitudinal primary vertex position from the VTX. The average beam position is calculated off line for each data acquisition run. This calculation yields a transverse profile of the Tevatron beam which is circular with a rms of ~25 μm in both the x- and y-directions. We find that the average beam trajectory is stable over the period that a given $p\bar{p}$ beam is stored in the

Tevatron Collider. A detailed description of the determination of the average beam line can be found in Ref. [15]. For the B_S^0 lifetime measurement, we consider only events from data runs with a sufficiently large number of collected events to allow a good determination of the run averaged beam line. In this analysis, we choose not to measure the primary vertex event-by-event because the presence of a second b quark decay in the event coupled with the low multiplicity in semileptonic B decays can lead to a systematic bias in the lifetime determination.

B. Decay length reconstruction

The tracks forming the D_S^- candidate are refit with a common vertex constraint referred to as the tertiary vertex $V_{D_S^-}$. The secondary vertex where the B_S^0 decays to a lepton and a D_S^- (referred to as $V_{B_S^0}$) is obtained by simultaneously intersecting the trajectory of the lepton track with the flight path of the D_S^- candidate. Since we fully reconstruct the D_S^- meson in the $\phi\pi^-$, $K^{*0}K^-$, and $K_S^0 K^-$ decay modes, we know the D_S^- flight path. In the $D_S^- \rightarrow \phi\mu^- \nu$ channel, where we do not fully reconstruct the D_S^- meson, we use the $\phi\mu^-$ flight direction as a good estimate of the D_S^- flight path.

The confidence level of the combined vertex fit is required to be greater than 1%. Furthermore, we require that the reconstructed D_S^- decay vertex $V_{D_S^-}$ be positively displaced from the primary vertex as projected along the direction of the D_S^- momentum.

The transverse decay length $L_{xy}(B_S^0)$ is defined as the displacement $\vec{X}$ in the transverse plane of $V_{B_S^0}$ from the primary event vertex projected onto the $D_S^- l^+$ momentum:

$$L_{xy}(B_S^0) = \frac{\vec{X} \cdot \vec{p_T}(D_S^- l^+)}{|\vec{p_T}(D_S^- l^+)|}. \tag{4}$$

L_{xy} is a signed variable which can be negative for the configuration where the particle seems to decay before the point where it is produced. The B_S^0 meson decay time is given by

$$ct(B_S^0) = L_{xy} \frac{m(B_S^0)}{p_T(B_S^0)}, \tag{5}$$

where $m(B_S^0)$ is the B_S^0 mass [1]. Since we do not fully reconstruct the B_S^0 meson in our analysis, we define the ''pseudo-proper decay length''

$$\lambda = L_{xy} \frac{m(B_S^0)}{p_T(D_S^- l^+)}, \tag{6}$$

which has a typical uncertainty of ~60 μm including the contribution from the finite size of the primary event vertex. In addition, we introduce a correction factor
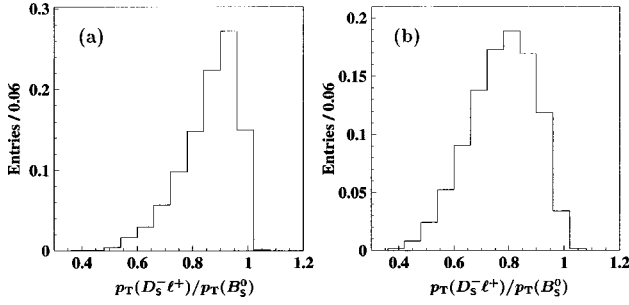
$$K = \frac{p_T(D_S^- l^+)}{p_T(B_S^0)}, \tag{7}$$

FIG. 2. Normalized K-factor distributions $p_T(D_S^- l^+)/p_T(B_S^0)$, for $B_S^0 \to D_S^- l^+ \nu X$ Monte Carlo decays with (a) $D_S^- \to \phi \pi^-$ and (b) $D_S^- \to \phi \mu^- \nu$.

to correct between the reconstructed $p_T(D_S^- l^+)$ and the unknown $p_T(B_S^0)$ in the data. The B_S^0 meson decay time is then given as

$$ct(B_S^0) = L_{xy} \frac{m(B_S^0)}{p_T(D_S^- l^+)} \times K. \qquad (8)$$

The correction between $p_T(D_S^- l^+)$ and $p_T(B_S^0)$ is done statistically by smearing an exponential decay distribution with a Monte Carlo distribution of the correction factor K when extracting $c\tau(B_S^0)$ from the pseudo-proper decay length in the lifetime fit as described in Sec. IV E. The K-distribution is obtained from $D_S^- l^+$ combinations which originate from a Monte Carlo simulation (see Sec. III D) of semileptonic B_S^0 decays into $D_S^{(*)-} l^+ X$ including $D_S^{(*)-} \tau^+ X$ with $\tau^+ \to l^+ X$. As an example, the K-distribution is shown for the $D_S^- \to \phi \pi^-$ and $D_S^- \to \phi \mu^- \nu$ decay modes in Figs. 2(a) and 2(b), respectively. The K-distributions have mean values of 0.86 and 0.77 with rms values of 0.10 and 0.12 for the $D_S^- \to \phi \pi^-$ and $D_S^- \to \phi \mu^- \nu$ modes, respectively. The K-distribution is approximately constant as a function of $p_T(D_S^- l^+)$ for the range of $p_T(D_S^- l^+)$ corresponding to our data.

To ensure a precise B_S^0 lifetime determination, we consider only B_S^0 candidates for which the pseudo-proper decay length is measured with an uncertainty of less than 0.1 cm. We also require that the D_S^- candidates have a proper decay length measured between $V_{B_S^0}$ and $V_{D_S^-}$ of less than 0.1 cm and that the uncertainty on this proper decay length be less than 0.1 cm. This requirement removes background events with very long-lived D_S^- candidates, where the long extrapolation back to the B_S^0 decay vertex results in a poor vertex measurement. These requirements have already been applied to the D_S^- mass distributions shown in Fig. 1.

C. Determination of the reflection from D^-

The reconstructions of the D_S^- decay modes into $K^{*0} K^-$ and $K_S^0 K^-$ suffer from reflections of $D^- \to K^{*0} \pi^-$ and $D^- \to K_S^0 \pi^-$, respectively, where the π^- is incorrectly assigned the kaon mass. We will discuss this reflection from D^- and the determination of the true number of events from the D_S^-
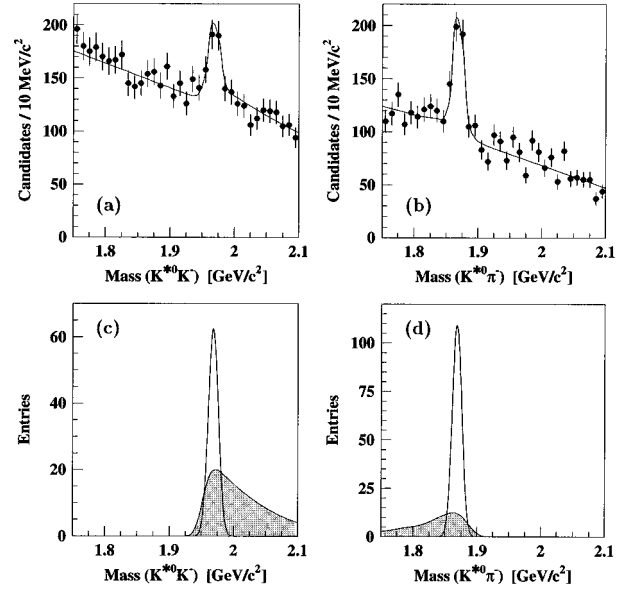

FIG. 3. (a) Mass distributions for candidates in the $D_S^- \to K^{*0} K^-$ decay mode. (b) Mass distribution if these candidates are assumed to be $D^- \to K^{*0} \pi^-$. (c) Distribution of the $D_S^- \to K^{*0} K^-$ signal and the reflection from $D^- \to K^{*0} \pi^-$ (shaded area) as obtained from Monte Carlo simulations. Normalizations are determined from the simultaneous fit described in the text. (d) Mass distribution of the corresponding $D^- \to K^{*0} \pi^-$ signal and the reflection from $D_S^- \to K^{*0} K^-$ (shaded area).

decay with the example of the $D_S^- \to K^{*0} K^-$ mode. The effect of this K-π misassignment can be seen in Fig. 3; events from a $B \to D^- l \nu X$ Monte Carlo simulation with $D^- \to K^{*0} \pi^-$ yield an invariant mass distribution indicated by the shape of the shaded area in Fig. 3(c) if they are reconstructed as $B_S^0 \to D_S^- l \nu X$ with $D_S^- \to K^{*0} K^-$, misinterpreting the π^- as K^-. A significant portion of this D^- reflection lies at the D_S^- mass peak.

Although we have already tightened our dE/dx likelihood ratio to better identify the K^- track as a kaon, CDF's dE/dx capabilities with a π/K separation of about 1σ for tracks with p_T greater than about 1 GeV/c are not sufficient to remove this D^- reflection. Applying a D^- mass veto by rejecting all $K^{*0} K^-$ combinations which are within a $\pm 3\sigma$ window around the nominal D^- mass when reconstructed as $K^{*0} \pi^-$ distorts the $K^{*0} K^-$ mass distribution. It would be very difficult to estimate the remaining D_S^- signal from that distribution and use it as input to the B_S^0 lifetime fit. We therefore choose to measure the D^- reflection directly from our data and account for the D^- component in the B_S^0 lifetime fit. We use two methods to determine the D^- reflection in our data.

The first method performs a simultaneous fit to the $K^{*0} K^-$ and $K^{*0} \pi^-$ invariant mass distributions, where the $K^{*0} \pi^-$ mass distribution is created by switching the mass assignment on the K^- track to be a pion. Figure 3(a) shows the $K^{*0} K^-$ mass distribution, while the corresponding $K^{*0} \pi^-$ mass distribution is displayed in Fig. 3(b). Each distribution is described by a Gaussian for the corresponding D^- and D_S^- signal as shown in Figs. 3(c) and 3(d) plus a

TABLE I. Summary of results for the four D_S^- decays: the number $N(D_S^-)$ of D_S^- signal events as input to the lifetime fit, the expected fraction f_{D_SD} of $B \to D_S^{(*)}D^{(*)}$ decays, the expected fraction $f_{D_SD_S}$ of $B_S^0 \to D_S^{(*)}D_S^{(*)}$ decays, the number N_{evt} of events in the signal samples, and the fitted B_S^0 lifetimes $c\tau(B_S^0)$, where the errors shown are statistical only.

D_S^- decay mode	$N(D_S^-)$	f_{D_SD}	$f_{D_SD_S}$	N_{evt}	$c\tau(B_S^0)$
$\phi\pi^-$	220 ± 21	2.6%	0.8%	350	418^{+43}_{-39} μm
$K^{*0}K^-$	125 ± 20	2.5%	0.8%	820	411^{+73}_{-66} μm
$K_S^0K^-$	33 ± 8	1.8%	0.6%	146	397^{+161}_{-152} μm
$\phi\mu^-\nu$	205 ± 38	5.7%	1.7%	635	399^{+50}_{-45} μm

linear line shape to parametrize the combinatorial background. The shape of the corresponding D^- or D_S^- reflection as obtained from a Monte Carlo simulation is also included in the fit as displayed in Figs. 3(c) and 3(d) as the shaded areas. The two mass distributions are fit simultaneously with the number of events in the Gaussian $D_S^-(D^-)$ signal constrained to the number of events in the corresponding D^- (D_S^-) reflection. In addition, the difference between the D_S^- and D^- mass values is fixed based on their nominal mass values [1]. The fit returns 123 ± 25 D_S^- signal events and 80 ± 10 events from the D^- reflection within the D_S^- signal region defined in Sec. IV E. The fit result is shown in Figs. 3(a)–3(d). We perform studies using MC pseudo-experiments to verify the validity of this method [19]. We find that the simultaneous fitting method returns the number of true D_S^- events in our MC studies with no bias and the error obtained from the fit to the data agrees with the expected uncertainty of this technique for our sample size.

The second method for determining the amount of D^- reflection in our D_S^- signal events exploits the difference between the D^- lifetime [$\tau(D^-)=(1.057 \pm 0.0015)$ ps [1]] and the D_S^- lifetime [$\tau(D_S^-)=(0.467 \pm 0.0017)$ ps [1]]. As described in Sec. IV F, we can determine the D_S^- lifetime in our fit for the B_S^0 lifetime. We modify the fitting method used to determine the D_S^- lifetime in the following way: We replace the exponential describing the D_S^- signal by the sum of two exponentials, one with the D_S^- lifetime and one with the D^- lifetime (see Sec. IV E about the fitting method and Sec. V for an example of a two-lifetime fit). We fix the D_S^- and D^- lifetimes to their nominal values [1] and allow the relative fractions of D_S^- and D^- to float in the fit. With this method we obtain 129^{+31}_{-34} D_S^- events and 84^{+34}_{-31} events attributed to the D^- reflection. We again perform studies using MC pseudo-experiments and verify the validity of this method to work without any bias [19].

We determine the weighted average of D_S^- events from both methods and obtain a D_S^- signal of 125 ± 20 events for the $D_S^- \to K^{*0}K^-$ decay. Both methods are also used to calculate the number of D_S^- events and the contribution from the D^- reflection in the $D_S^- \to K_S^0K^-$ decay mode. We obtain 33 ± 8 D_S^- signal events for the $K_S^0K^-$ mode. These numbers are displayed in Table I together with the numbers of D_S^- signal events for the $D_S^- \to \phi\pi^-$ and $D_S^- \to \phi\mu^-\nu$ decay

modes. As further described in Sec. IV E, these event numbers are used as a constraint in the B_S^0 lifetime fit.

D. Non-B_S^0 background

There are two possible sources of non-strange B meson decays which can lead to "right-sign" $D_S^-l^+$ combinations. The first process originates from the decays $\bar{B}^0 \to D_S^{(*)-}D^{(*)+}X$ and $B^- \to D_S^{(*)-}D^{(*)0}X$, with the D^0 or D^+ decaying semileptonically. These decays produce softer and less isolated leptons than the leptons from B_S^0 semileptonic decays. Therefore we expect the acceptance for this background source relative to the B_S^0 signal to be quite small. We use a Monte Carlo simulation of these events and estimate their contribution f_{D_SD} in the following way:

$$f_{D_SD} = \epsilon_{\text{rel}} \frac{f_u + f_d}{f_S} \frac{\mathcal{B}(B \to D_S^{(*)}D^{(*)}X)}{\mathcal{B}(B_S^0 \to D_S^{(*)}l\nu X)}. \tag{9}$$

We use the following branching ratios and fragmentation fractions from the Particle Data Group [1]: $\mathcal{B}(B_S^0 \to D_s^{(*)}l\nu X)=(7.6 \pm 2.4)\%$, $\mathcal{B}(B \to D_S^{(*)}D^{(*)}X)=(4.9 \pm 1.1)\%$, $f_u=f_d=(37.8 \pm 2.2)\%$, and $f_S=(11.2 \pm 2.2)\%$. Here ϵ_{rel} is the ratio of efficiencies and acceptances for both decays obtained from a Monte Carlo simulation:

$$\epsilon_{\text{rel}} = \frac{\epsilon(B \to D_S^{(*)}D^{(*)}X)}{\epsilon(B_S^0 \to D_S^{(*)}l\nu X)}. \tag{10}$$

The values obtained for ϵ_{rel} are in the order of 0.5%–1%. The calculated fractions f_{D_SD} for each D_S^- decay mode are compiled in Table I. The f_{D_SD} fraction is larger for the $D_S^- \to \phi\mu^-\nu$ decay mode because of the on average softer B meson momentum in the dimuon data sample compared to the single lepton trigger events.

The second process is a four body decay $B^0/B^+ \to D_S^-\mathcal{K}l^+\nu X$, where $\mathcal{K}$ denotes any type of strange meson. Because of the low probability of producing $s\bar{s}$ pairs and the limited phase space, this process is suppressed and has not been observed experimentally [20]. Based on the quoted limit $\mathcal{B}(B^0/B^+ \to D_S^-l^+\nu X)<0.9\%$ (90% C.L.) [1,20] and our detection efficiency determined from MC simulation, we expect less than 1.0% of our $D_S^-l^+$ combinations to originate from this source.

We also consider events from $B_S^0 \to D_S^{(*)+}D_S^{(*)-}X$ decays, with one D_S decaying semileptonically. This contribution to our B_S^0 lifetime sample is determined from Monte Carlo studies in the same way as described above for the $B \to D_S^{(*)}D^{(*)}X$ background. The obtained fractions $f_{D_SD_S}$ from these decays are small and compiled in Table I. Finally, backgrounds with a real D_S^- meson and a fake lepton from decays such as $B \to D_S^{(*)}D^{(*)}X$ with a hadron from the $D^{(*)}$ decay faking a lepton are negligible due to the low probability of a hadron faking a lepton.

In summary, the contribution of all above physics backgrounds is quite small compared to the combinatorial back-

ground. We account for contributions from $B \rightarrow D_S^{(*)} D^{(*)} X$ and $B_S^0 \rightarrow D_S^{(*)+} D_S^{(*)-} X$ decays in our lifetime fit described next, and treat the contribution of $B^0/B^+ \rightarrow D_S^- \mathcal{K} l^+ \nu X$ decays as a source of systematic uncertainty in the B_S^0 lifetime measurement.

E. Description of the lifetime fit

As input to the B_S^0 lifetime fit, we define a signal sample using a D_S^- mass window from 1.944 GeV/c^2 to 1.994 GeV/c^2 for the $D_S^- \rightarrow \phi \pi^-$, $K^{*0} K^-$, and $K_S^0 K^-$ decay modes and a ϕ signal window from 1.0094 GeV/c^2 to 1.0294 GeV/c^2 for the $D_S^- \rightarrow \phi \mu^- \nu$ decay channel. The numbers of events in the signal samples can be found for the four decay modes in Table I. To model the pseudo-proper decay length distribution of the combinatorial background events contained in the signal sample, we define a background sample which consists of ''right-sign'' events from the D_S^- sidebands (1.884–1.934 GeV/c^2 and 2.004–2.054 GeV/c^2) and ''wrong-sign'' events from the interval 1.884–2.054 GeV/c^2. For the $D_S^- \rightarrow \phi \mu^- \nu$ decay mode the ϕ sidebands are defined from 0.9844–1.0044 GeV/c^2 and from 1.0344 GeV/c^2–1.0544 GeV/c2, while the ''wrong-sign'' combinations are taken from the region 0.9844 GeV/c^2–1.0544 GeV/c^2. We assume the combinatorial background to originate from random track combinations and therefore use the sidebands to model the background in the signal sample. This assumption is supported by the mass distribution of the ''wrong-sign'' combinations where no enhancement is visible at the D_S^- mass. By adding the ''wrong-sign'' combinations to the ''right-sign'' sideband events, we better constrain the shape of the combinatorial background events in the D_S^- signal samples for decay channels with low combinatorial background like the $D_S^- \rightarrow \phi \pi^-$ mode.

The pseudo-proper decay length distribution obtained from the signal sample is fit using an unbinned maximum log-likelihood method. Both the B_S^0 lifetime, denoted as $c \tau$ below, and the background shape are determined in a simultaneous fit using the signal and background samples. Thus the likelihood function $\mathcal{L}$ is a combination of two parts:

$$\mathcal{L} = \prod_i^{N_S} [f_{\text{sig}} \mathcal{F}_{\text{sig}}^i + (1 - f_{\text{sig}}) \mathcal{F}_{\text{bg}}^i] \prod_j^{N_B} \mathcal{F}_{\text{bg}}^j, \quad (11)$$

where N_S and N_B are the number of events in the signal and background samples. f_{sig} is the ratio of D_S^- signal events obtained from the D_S^- mass distributions (see Table I) to the total number of events in the signal sample. To constrain f_{sig} we factor in an additional χ^2 term to the likelihood function $\mathcal{L}$ above to constrain the number of D_S^- signal events obtained from the invariant mass distributions within their uncertainty.

The signal probability function $\mathcal{F}_{\text{sig}}$ consists of a normalized decay exponential function convoluted with a Gaussian resolution function $\mathcal{G}$ and is smeared with a normalized K-distribution $\mathcal{H}(K)$:

$$\mathcal{F}_{\text{sig}}^i(x) = \int dK \, \mathcal{H}(K) \left[\frac{K}{c\tau} \exp\left\{ -\frac{Kx}{c\tau} \right\} \otimes \mathcal{G}(\lambda^i | x, s\sigma^i) \right]. \quad (12)$$

Here, λ^i is the measured pseudo-proper decay length with uncertainty σ^i and x is the true pseudo-proper decay length. Because of systematic uncertainties in the overall scale of the decay length uncertainties, which we estimate on an event-by-event basis, we introduce a scale factor, s, which is a free parameter in the B_S^0 lifetime fit. We subsequently vary s in the fits to determine the sensitivity of our measurement to this uncertainty. The integration over the momentum ratio K is approximated by a finite sum

$$\int dK \, \mathcal{H}(K) \rightarrow \sum_i \, \Delta K \, \mathcal{H}(K_i), \quad (13)$$

where the sum is taken over bin i of a histogrammed distribution $\mathcal{H}(K_i)$ with bin width ΔK as shown e.g. in Fig. 2.

The background probability function $\mathcal{F}_{\text{bg}}$ is parametrized by a Gaussian centered at zero, a negative exponential tail, and a positive decay exponential to characterize the contribution of heavy flavor decays in the background sample:

$$\mathcal{F}_{\text{bg}}^i(x) = (1 - f_+ - f_-) \mathcal{G}(\lambda^i | x, s\sigma^i)$$
$$+ \frac{f_+}{\lambda_+} \exp\left\{ -\frac{x}{\lambda_+} \right\} \otimes \mathcal{G}(\lambda^i | x, s\sigma^i)$$
$$+ \frac{f_-}{\lambda_-} \exp\left\{ -\frac{x}{\lambda_-} \right\} \otimes \mathcal{G}(\lambda^i | x, s\sigma^i). \quad (14)$$

Here, $f_\pm$ are the fractions of positive and negative lifetime backgrounds and $\lambda_\pm$ are the effective lifetimes of those backgrounds. We verify the parameters $f_\pm$ and $\lambda_\pm$ agree with the ''right-sign'' sideband events and the ''wrong-sign'' combinations separately, allowing us to combine both samples resulting in the background samples described above.

The events originating from the D^- reflection in the $D_S^- \rightarrow K^{*0} K^-$ and $D_S^- \rightarrow K_S^0 K^-$ decays (see Sec. IV C) are also accounted for in the likelihood function by a term

$$\int dK \, \mathcal{H}(K) \left[f_{D^-} \frac{K}{c\tau(B)} \exp\left\{ -\frac{Kx}{c\tau(B)} \right\} \otimes \mathcal{G}(\lambda^i | x, s\sigma^i) \right], \quad (15)$$

where f_{D^-} refers to the fraction of the D^- reflection in the D_S^- sample and $c\tau(B)$ is taken to be the world average B^0 lifetime [1].

F. Fit results

We first determine the B_S^0 lifetime for each of the four D_S^- decay channels individually. The parameters allowed to float in the fit are the B_S^0 lifetime, $f_{\text{sig}}, \lambda_\pm, f_\pm$, and the overall scale factor s. The fitted values for $c\tau(B_S^0)$ and their statistical uncertainties are shown in Table I, and are in good statistical agreement. The pseudo-proper decay length distribution of the signal sample with the result of the fit
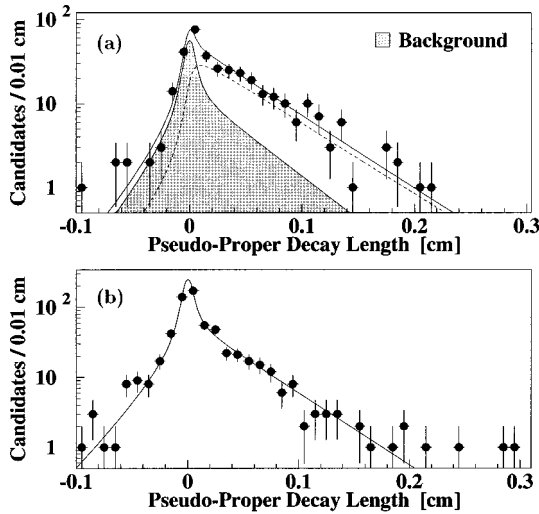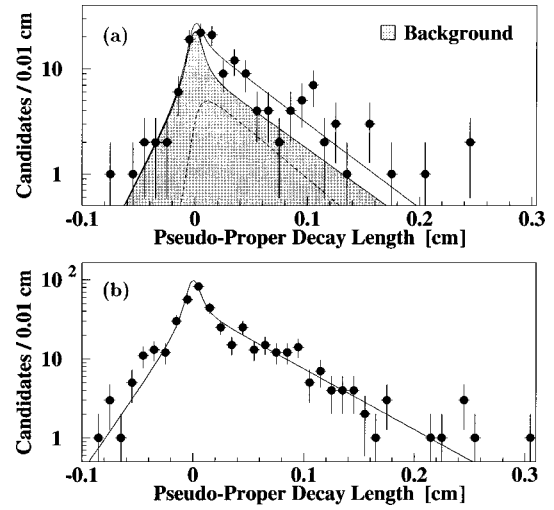
FIG. 4. (a) B_S^0 pseudo-proper decay length distribution for the $D_S^- \to \phi \pi^-$ signal sample with the result of the fit superimposed. The dashed line is the B_S^0 signal contribution, while the shaded curve represents the contribution from the combinatorial background. (b) Pseudo-proper decay length distribution for the background sample with the fit result superimposed.

superimposed is shown in Fig. 4(a) for the $D_S^- \to \phi \pi^-$ decay mode. The dashed line represents the B_S^0 signal contribution, while the shaded curve shows the sum of the background probability function over the events in the signal sample. The same distribution of the background sample is displayed in Fig. 4(b) with the result of the fit superimposed. Figures 5, 6, and 7 show the corresponding distributions for the $D_S^- \to K^{*0}K^-$, $D_S^- \to K_S^0 K^-$, and $D_S^- \to \phi \mu^- \nu$ decay modes, respectively. The combined B_S^0 lifetime from all four D_S^- decay modes is determined from a simultaneous fit to be

$c \tau(B_S^0) = (408^{+28}_{-27})$ μm or $\tau(B_S^0) = (1.36 \pm 0.09)$ ps, where the errors shown are statistical only.

As a consistency check, we use the $D_S^- \to \phi \pi^-$ decay mode to also fit the D_S^- lifetime from the proper decay length measured from the secondary vertex V_{B_S} to the tertiary vertex V_{D_S}. Since the D_S^- decay is fully reconstructed, its relativistic boost is known and a convolution with a p_T-correction factor distribution in the fit does not apply. The result is $c \tau(D_S^-) = (136^{+17}_{-15})$ μm (statistical error only), which is consistent with the world average D_S^- lifetime [1].
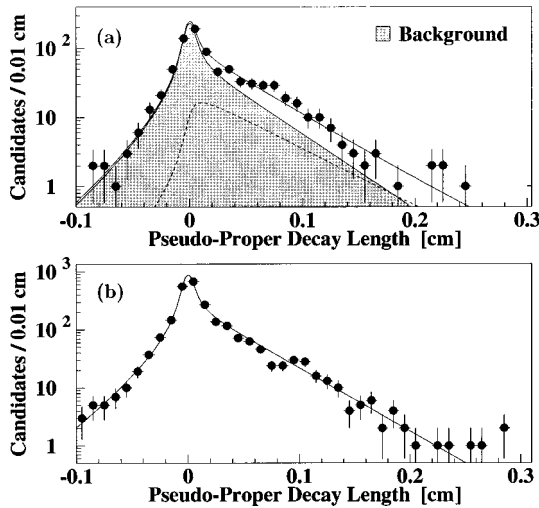

FIG. 5. (a) B_S^0 pseudo-proper decay length distribution for the $D_S^- \to K^{*0}K^-$ signal sample with the result of the fit superimposed. The dashed line is the B_S^0 signal contribution, while the shaded curve represents the contribution from the combinatorial background. (b) Pseudo-proper decay length distribution for the background sample with the fit result superimposed.
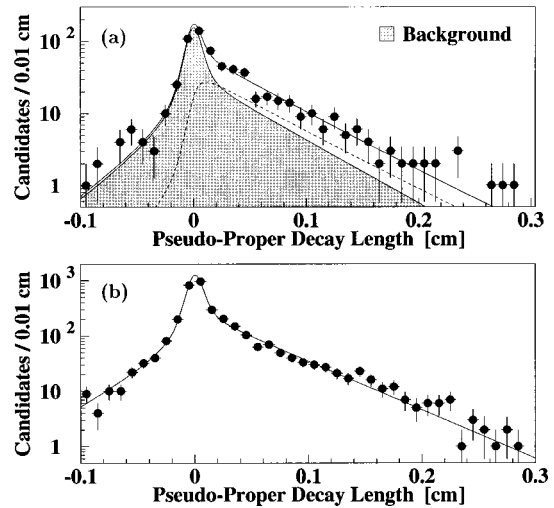

FIG. 6. (a) B_S^0 pseudo-proper decay length distribution for the $D_S^- \to K_S^0 K^-$ signal sample with the result of the fit superimposed. The dashed line is the B_S^0 signal contribution, while the shaded curve represents the contribution from the combinatorial background. (b) Pseudo-proper decay length distribution for the background sample with the fit result superimposed.
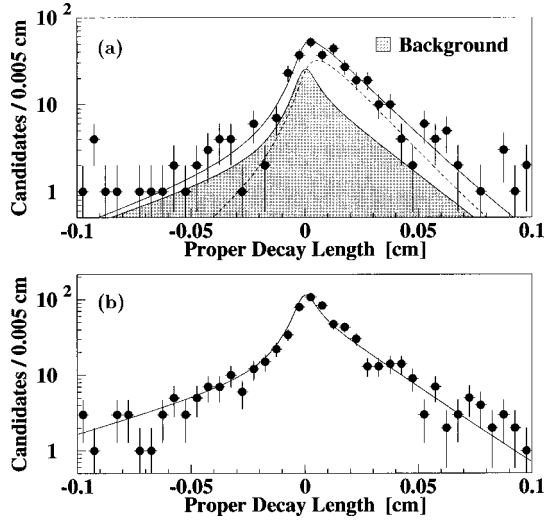

FIG. 7. (a) B_S^0 pseudo-proper decay length distribution for the $D_S^- \to \phi \mu^- \nu$ signal sample with the result of the fit superimposed. The dashed line is the B_S^0 signal contribution, while the shaded curve represents the contribution from the combinatorial background. (b) Pseudo-proper decay length distribution for the background sample with the fit result superimposed.

FIG. 8. (a) D_S^- proper decay length distribution $c\tau(D_S^-)$ for the $D_S^- \to \phi\pi^-$ signal sample with the result of the fit superimposed. The dashed line is the D_S^- signal contribution, while the shaded curve represents the contribution from the combinatorial background. (b) Proper decay length distribution $c\tau(D_S^-)$ for the background sample with the fit result superimposed.

Figures 8(a) and 8(b) show the D_S^- proper decay length distributions for the signal and background samples, respectively, with the results of the fit superimposed.

G. Systematic uncertainties

Table II lists all sources of systematic uncertainty considered in this analysis. The major contribution originates from the treatment of the background. In particular, the following evaluations of systematic errors are performed yielding the uncertainties reported in Table II:

Background treatment: The combinatorial background in the signal sample is parametrized by the positive and negative lifetimes λ_+ and λ_- as well as their respective fractions f_+ and f_- as described in Eq. (14). To evaluate the depen-

TABLE II. Compilation of systematic uncertainties in the measurement of the B_S^0 lifetime combining all four D_S^- decay modes.

Error source	$\Delta c\tau(B_S^0)$
Background treatment	± 11 μm
Non-B_S^0 backgrounds	± 6 μm
Decay length requirement	$^{+1}_{-5}$ μm
Momentum estimate	
Lepton p_T dependence	$^{+6}_{-3}$ μm
B decay model	$^{+3}_{-1}$ μm
b quark p_T spectrum	± 5 μm
Electron selection	± 3 μm
Decay length resolution	$^{+7}_{-2}$ μm
D^- reflection	± 1 μm
Detector alignment	± 2 μm
Total	$^{+17}_{-15}$ μm

dence of the B_S^0 lifetime on the background parametrization, we vary $\lambda_\pm$ and $f_\pm$ within $\pm 1\sigma$ of their values returned from the B_S^0 lifetime fit. Since there is a correlation between the background parameters $\lambda_\pm$ and $f_\pm$ and the B_S^0 lifetime in the simultaneous fit to the signal and background samples, part of this systematic uncertainty is already accounted for in the statistical error on $\tau(B_S^0)$. However, this correlation is small. We therefore adopt this method as a conservative way to evaluate the systematic uncertainty from background treatment.

Non-B_S^0 backgrounds: These backgrounds (see Sec. IV D) enter our fit as fixed fractions. We vary these fractions within $\pm 50\%$ of their reported values (see Table I) and repeat the fit. We also evaluate the background from $B^0/B^+ \to D_S^- \mathcal{K}l^+ \nu X$ decays and consider its fraction to be 2.0%, twice the quoted limit [1,20].

Decay length requirement: There are two requirements that can bias the B_S^0 lifetime result. These are the cut on $|c\tau(D_S^-)| < 0.1$ cm and the requirement that the reconstructed D_S^- decay vertex $V_{D_S^-}$ be positively displaced from the primary event vertex. To study the effect of these cuts, we use high statistics Monte Carlo samples. We first fit the lifetime with all the selection requirements, and then remove each cut individually noting the shift in the B_S^0 lifetime.

Momentum estimate: The B_S^0 lifetime result is sensitive to the distribution of the correction factor $\mathcal{H}(K)$, which can be affected by the lepton p_T cut and the decay kinematics. For the standard fit we require $p_T(\mu) > 2.0$ GeV/c for the $D_S^- \to \phi\mu^- \nu$ decay mode and $p_T(l) > 6.0$ GeV/c for the other D_S^- decay channels. To test the effect of the lepton p_T dependence, we generate new K-distributions for lower and higher lepton p_T cut values. We also compare the effect on the kinematics of semileptonic B_S^0 decays using a pure V-A decay versus semileptonic decays using the ISGW form factor [21]. In addition, an alternative p_T spectral shape of b quark production is considered based on a comparison of the lepton p_T shape in the data and in Monte Carlo events. Finally, the K-distribution is somewhat dependent on the electron identification. We study a possible incompleteness in the treatment of the electron selection with our Monte Carlo simulation and assign a systematic error of ± 3 μm.

Decay length resolution: Our uncertainty on the estimate of the decay length resolution is expressed in the scale factor s, which is fitted to 1.29 ± 0.03. We fix the scale factor at 1.0, and again at 1.38, the latter corresponding to a $+3\sigma$ upward shift from the fitted value, and repeat the B_S^0 lifetime fit.

D^- reflection: The reflection from D^- in the $D_S^- \to K^{*0}K^-$ and $D_S^- \to K_S^0 K^-$ decay modes changes the number of D_S^- signal events in these two channels. We study the influence of the D^- reflection by varying the number of D_S^- signal events within their error as determined in Sec. IV C.

Detector alignment: We also account for a possible residual misalignment of the SVX and assign an error of ± 2 μm as further detailed in Ref. [15].

The systematic uncertainties noted above have been combined in quadrature. Quoting the statistical and systematic

uncertainties separately, we measure the B_S^0 lifetime using semileptonic B_S^0 decays to be

$$\tau(B_S^0) = (1.36 \pm 0.09^{+0.06}_{-0.05}) \text{ ps}, \tag{16}$$

where the first error is statistical and the second systematic. This result is currently the world's best measurement of the B_S^0 lifetime from a single experiment. In comparison, the world average B_S^0 lifetime is (1.57 ± 0.08) ps [1]. This measurement supersedes CDF's previously published B_S^0 lifetime result of $\tau(B_S^0) = (1.42^{+0.27}_{-0.23} \pm 0.11)$ ps using a data sample corresponding to an integrated luminosity of 20 pb^{-1} [5].

Using the CDF average B^0 lifetime $\tau(B^0) = (1.513 \pm 0.053)$ ps [22], we determine the B_S^0/B^0 lifetime ratio to be 0.899 ± 0.072, taking correlated systematic uncertainties into account. However, ignoring the correlated systematic uncertainties increases the error on the B_S^0/B^0 lifetime ratio only to ± 0.077, since $\tau(B_S^0)/\tau(B^0)$ is dominated by the statistical error on the B_S^0 lifetime measurement.

V. DETERMINATION OF $\Delta\Gamma/\Gamma$

We examine the B_S^0 meson pseudo-proper decay length distribution from $D_S^- l^+$ correlations for a lifetime difference $\Delta\Gamma/\Gamma$ between the two mass eigenstates of the B_S^0 meson, B_S^H and B_S^L. In the case of a lifetime difference in the B_S^0 system, the decay length distribution for events from the semileptonic decay $B_S^0 \to D_S^- l^+ \nu X$ is expected to be governed by the sum of two exponentials. We expand the likelihood fit to describe the B_S^0 pseudo-proper decay length distribution to a function of the form

$$\mathcal{F}(t) = e^{-\Gamma_H t} + e^{-\Gamma_L t}$$

$$\text{with } \Gamma_{L,H} = \Gamma \pm \frac{\Delta\Gamma}{2} = \Gamma \left(1 \pm \frac{1}{2} \frac{\Delta\Gamma}{\Gamma} \right), \tag{17}$$

rather than fitting for just one exponential lifetime $e^{-\Gamma t}$. The parameter $\Delta\Gamma/\Gamma$ is the parameter we fit for. Since $\Delta\Gamma/\Gamma$ is symmetric about zero, it is required to be positive. In the case of a lifetime difference $\Delta\Gamma \neq 0$, the total decay width $\Gamma = \frac{1}{2}(\Gamma_H + \Gamma_L)$ and the mean B_S^0 lifetime $\tau_m(B_S^0)$ obtained from a fit assuming a single B_S^0 lifetime are no longer reciprocal to each other but follow the relation

$$\tau_m(B_S^0) = \frac{1}{\Gamma} \frac{1 + (\Delta\Gamma/2\Gamma)^2}{1 - (\Delta\Gamma/2\Gamma)^2}. \tag{18}$$

We incorporate the relation in Eq. (18) into our likelihood fitting function. We follow the suggestion given in Ref. [9] and fix the mean B_S^0 lifetime to the world average B^0 lifetime since both lifetimes are expected to agree within 1% [2,3]. This theoretical assumption can be verified by the current world average $\tau(B^0) = (1.55 \pm 0.05)$ ps and $\tau(B_S^0) = (1.57 \pm 0.08)$ ps. The CDF average B_S^0/B^0 lifetime ratio derived above also supports this assumption.

The fit returns $\Delta\Gamma/\Gamma = 0.34^{+0.31}_{-0.34}$, where the given error is statistical only. This indicates that with the current statistics

of our $D_S^- l^+$ sample we are not sensitive to a B_S^0 lifetime difference. Based on this fit result, we integrate the normalized likelihood as a function of $\Delta\Gamma/\Gamma$ and find the 95% confidence level (C.L.) limit at

$$\frac{\Delta\Gamma}{\Gamma} < 0.83 \quad (95\% \text{ C.L.}). \tag{19}$$

This is the first experimental result for the lifetime difference in the B_S^0 system.

Using a value of $\Delta\Gamma/\Delta m = (5.6 \pm 2.6) \times 10^{-3}$ from Ref. [9] and setting $\tau_m(B_S^0)$ to the world average B^0 lifetime [1], an upper limit on the B_S^0 mixing frequency of $\Delta m_S < 96$ ps^{-1} (95% C.L.) can be determined within the standard model. Including the dependence on $\Delta\Gamma/\Delta m$ and $\tau_m(B_S^0)$ in our limit, we obtain

$$\Delta m_S < 96 \text{ ps}^{-1} \times \left(\frac{5.6 \times 10^{-3}}{\Delta\Gamma/\Delta m} \right) \left(\frac{1.55 \text{ ps}}{\tau_m(B_S^0)} \right) \quad (95\% \text{ C.L.}). \tag{20}$$

VI. CONCLUSION

We have presented a measurement of the B_S^0 meson lifetime using semileptonic B_S^0 decays, where the D_S^- meson is reconstructed through the four decay modes $D_S^- \to \phi\pi^-, D_S^- \to K^{*0}K^-, D_S^- \to K_S^0 K^-$, and $D_S^- \to \phi\mu^-\nu$. We obtain

$$\tau(B_S^0) = (1.36 \pm 0.09^{+0.06}_{-0.05}) \text{ ps}, \tag{21}$$

where the first error is statistical and the second systematic. This is currently the world's best measurement of the B_S^0 lifetime from a single experiment. This result agrees with an earlier CDF measurement [5], which is superseded by the present measurement. We determine the B_S^0/B^0 lifetime ratio to be 0.899 ± 0.072 using the CDF average B^0 lifetime [22].

In addition, we have examined the B_S^0 meson pseudo-proper decay length distribution for a lifetime difference $\Delta\Gamma/\Gamma$ between the two mass eigenstates of the B_S^0 meson, B_S^H and B_S^L. Using all four D_S^- decay modes, an upper limit of $\Delta\Gamma/\Gamma < 0.83$ is set at 95% C.L., corresponding to the standard model limit

$$\Delta m_S < 96 \text{ ps}^{-1} \times \left(\frac{5.6 \times 10^{-3}}{\Delta\Gamma/\Delta m} \right) \left(\frac{1.55 \text{ ps}}{\tau_m(B_S^0)} \right) \quad (95\% \text{ C.L.}). \tag{22}$$

With considerably increased statistics in the next run of the Tevatron Collider, our sensitivity to the lifetime difference $\Delta\Gamma/\Gamma$ will be significantly improved [23].

[1] Particle Data Group, R.M. Barnett *et al.*, Phys. Rev. D **54**, 1 (1996), and 1997 off-year partial update for the 1998 edition available on the PDG WWW pages (URL: http://pdg.lbl.gov/).

[2] M.B. Voloshin and M.A. Shifman, Sov. Phys. JETP **64**, 698 (1986); I.I. Bigi and N.G. Uraltsev, Phys. Lett. B **280**, 271 (1992); I.I. Bigi, Nuovo Cimento A **109**, 713 (1996).

[3] M. Neubert, Int. J. Mod. Phys. A **11**, 4173 (1996); M. Neubert and C.T. Sachrajda, Nucl. Phys. **B483**, 339 (1997).

[4] ALEPH Collaboration, D. Buskulic *et al.*, Z. Phys. C **69**, 585 (1996); Phys. Lett. B **377**, 205 (1996); CDF Collaboration, F. Abe *et al.*, Phys. Rev. Lett. **77**, 1945 (1996); DELPHI Collaboration, P. Abreu *et al.*, Z. Phys. C **71**, 11 (1996); OPAL Collaboration, R. Akers *et al.*, Phys. Lett. B **350**, 273 (1995); OPAL Collaboration, K. Ackerstaff *et al.*, Eur. Phys. J. C **2**, 407 (1998); Phys. Lett. B **426**, 161 (1998).

[5] CDF Collaboration, F. Abe *et al.*, Phys. Rev. Lett. **74**, 4988 (1995).

[6] S.L. Glashow, Nucl. Phys. **22**, 579 (1961); S. Weinberg, Phys. Rev. Lett. **19**, 1264 (1967); A. Salam, in *Elementary Particle Theory*, edited by N. Svartholm (Almquist and Wiksells, Stockholm, 1969), p. 367.

[7] I. Bigi *et al.*, in *B Decays*, 2nd edition, edited by S. Stone (World Scientific, Singapore, 1994), p. 132.

[8] I. Dunietz, Phys. Rev. D **52**, 3048 (1995).

[9] M. Beneke, G. Buchalla, and I. Dunietz, Phys. Rev. D **54**, 4419 (1996).

[10] N. Cabibbo, Phys. Rev. Lett. **10**, 531 (1963); M. Kobayashi and T. Maskawa, Prog. Theor. Phys. **49**, 652 (1973).

[11] J. Hagelin, Nucl. Phys. **B193**, 123 (1981); V.A. Khoze, M.A. Shifman, N.G. Uraltsev, and M.B. Voloshin, Sov. J. Nucl. Phys. **46**, 112 (1987); A. Datta, E.A. Paschos, and U. Türke, Phys. Lett. B **196**, 382 (1987); I. Dunietz, Ann. Phys. (N.Y.) **184**, 350 (1988).

[12] CDF Collaboration, F. Abe *et al.*, Nucl. Instrum. Methods Phys. Res. A **271**, 387 (1988), and references therein.

[13] D. Amidei *et al.*, Nucl. Instrum. Methods Phys. Res. A **350**, 73 (1994); P. Azzi *et al.*, *ibid.* **360**, 137 (1995).

[14] G.W. Foster, J. Freeman, C. Newman-Holmes, and J. Patrick, Nucl. Instrum. Methods Phys. Res. A **269**, 93 (1988).

[15] CDF Collaboration, F. Abe *et al.*, Phys. Rev. D **57**, 5382 (1998).

[16] P. Nason, S. Dawson, and R.K. Ellis, Nucl. Phys. **B327**, 49 (1989); M.L. Mangano, P. Nason, and G. Rudolfi, *ibid.* **B373**, 295 (1992).

[17] A.D. Martin, W.J. Stirling, and R.G. Roberts, Phys. Rev. D **47**, 867 (1993).

[18] C. Peterson, D. Schlatter, I. Schmitt, and P. Zerwas, Phys. Rev. D **27**, 105 (1983).

[19] K. Burkett, Ph.D. thesis, University of Michigan, 1998.

[20] ARGUS Collaboration, H. Albrecht *et al.*, Z. Phys. C **60**, 11 (1993).

[21] N. Isgur, D. Scora, B. Grinstein, and M.B. Wise, Phys. Rev. D **39**, 799 (1989).

[22] CDF Collaboration, F. Abe *et al.*, Phys. Rev. D **58**, 092002 (1998).

[23] CDF Collaboration, R. Blair *et al.*, The CDF II Detector: Technical Design Report No. Fermilab-Pub-96-390-E, 1996.